Spectrochimica Acta Part A: Molecular and Biomolecular Spectroscopy 300 (2023) 122899

Contents lists available at ScienceDirect

Spectrochimica Acta Part A:
Molecular and Biomolecular Spectroscopy

journal homepage: www.journals.elsevier.com/spectrochimica-acta-part-a-molecular-and-biomolecular-spectroscopy

Sulfites detection by surface-enhanced Raman spectroscopy: A feasibility study

Alberto Villar [a,*], Santos Merino [a,b], Roberto A. Boto [c,d], Javier Aizpurua [c,d], Aitzol Garcia [c,d], Mikel Azkune [e], Joseba Zubia [f]

[a] Surface Chemistry Unit, Tekniker, Basque Research and Technology Alliance (BRTA), C/Iñaki Goenaga 5, 20600 Eibar, Spain
[b] Departamento de Electricidad y Electrónica Universidad del País Vasco, UPV/EHU, Leioa 48940, Spain
[c] Theory of Nanophotonics Group, Materials Physics Center (CSIC-UPV/EHU), Donostia-San Sebastián, Spain
[d] Donostia International Physics Center, Paseo Manuel Lardizabal 4, 200018 Donostia-San Sebastian, Spain
[e] Department of Electronic Technology, Engineering School of Bilbao, University of the Basque Country (UPV/EHU), Torres Quevedo 1, E-48013 Bilbao, Spain
[f] Department of Communications Engineering, Engineering School of Bilbao, University of the Basque Country (UPV/EHU), Plaza Ingeniero Torres Quevedo, 1, E-48013 Bilbao, Spain

HIGHLIGHTS

- A feasibility study of a new methodology for free SO_2 monitoring based on SERS.
- Theoretical study to identify the Raman active vibrational modes.
- Development of a laboratory SERS method that can be easy transferable to the field.
- Multivariate calibration procedure for free SO_2 quantification by chemometrics.

GRAPHICAL ABSTRACT

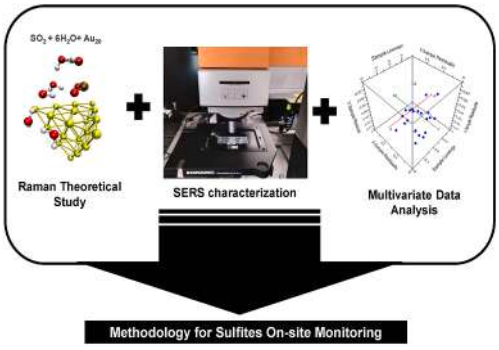

ARTICLE INFO

Keywords:
Sulfites
Wine
Modelling
Surface-enhanced Raman spectroscopy
Chemometrics

ABSTRACT

The exhaustive control required for the correct wine production needs of many chemical analysis throughout the process. The most extended investigations for wine production control are focused on the quantification of total and free SO_2. Most methods described in the literature have an adequate detection limit, but they usually lack reproducibility and require a previous sample treatment for the extraction of the SO_2 from the wine-matrix. In this context, Surface-Enhanced Raman Spectroscopy (SERS) can be a promising technique for free SO_2 determination without the need for any sample pre-processing. This work describes a proof of concept of a new methodology based on SERS and supported by Density Functional Theory (DFT) calculations to identify the active vibrational modes of the key molecules that contribute to the concentration of free SO_2 in solution. Theoretical predictions and experimental outcomes are brought together to chemometrics to get a simple and real-time free SO_2 monitoring. This general procedure could pave the way towards an implementation of a portable SERS detection module for in-field measurements.

* Corresponding author.
E-mail address: alberto.villar@tekniker.es (A. Villar).

https://doi.org/10.1016/j.saa.2023.122899
Received 20 January 2023; Received in revised form 5 May 2023; Accepted 17 May 2023
Available online 20 May 2023

1. Introduction

Sulfites are a group of sulfur-based compounds used for centuries to preserve wine and other foods. These compounds have been applied since the ancient Romans to prevent the transformation of wine into vinegar, and nowadays they are still used at different stages of the wine production process due to their low cost and antimicrobial/antioxidant properties. Sulfites are commonly added as gaseous sulfur dioxide (SO_2) dissolved in water (European food additive number E220), potassium bisulfite (European food additive number E228) or potassium-metabisulfite (European food additive number E224), although SO_2 is also generated in small concentrations during fermentation process as a metabolic intermediate of the sulfate reduction pathway. During the vinification process, the different chemical forms of SO_2 are known as free or combined. The second one is more abundant than free SO_2, but it has less antioxidant properties. Free SO_2 is the gaseous and inorganic fraction, while combined SO_2 is the fraction linked to different organic substances in wine such as acetaldehyde. Both fractions are in equilibrium depending on the pH, temperature, and composition of the wine. The sum of both fractions is described as total SO_2. Free SO_2 is the sum of molecular sulfur dioxide (SO_2), bisulfite ion (HSO_3^-) and sulfite ion (SO_3^{2-}), where molecular SO_2 is the so-called active form, and the concentration of each one of the species in equilibrium depends on the pH [23,7]. The application of excessive SO_2 must be avoided because it produces undesired organoleptic reactions in the final product. On the other hand, insufficient concentration of SO_2 does not protect the wine against excessive oxidation or microbiological processes that affect wine's quality. From a health perspective, sulfites have been related to asthmatic reactions, breathing difficulties or diarrhoea in a subset of the population, mainly in asthmatics and in children [21,13]. In this context, the final SO_2 concentration in wine was limited by the International Organisation of Vine and Wine (OIV) at 400 mg/l for white wines and 150 mg/l for red wines.

The most common international standard methods (Compendium of International Methods of Wine and Must Analysis-OIV) for the determination of sulfites in wine are the Moinier-Williams method (OIV-MA-AS323-04A) and the iodometric Ripper method (OIV-MA-AS323-04B). The first one is an acid-base titration method that requires the conversion of sulfites to SO_2 gas. This method, which is time-consuming, depends on the analyst's skills and requires a large volume of sample. In the second method, free sulfur dioxide concentration is determined by direct titration with iodine and the combined sulfur dioxide concentration is determined by iodometric titration after alkaline hydrolysis. This method is affected by the matrix and shows reproducibility problems. There are other standard methods based on electrochemical enzymatic detection [43] or an ion exclusion chromatographic method (AOAC official method 990.31), but both are too expensive and time-consuming. The relevant literature shows examples of alternative methods applied for sulfites quantification in wine based on *para*-rosaniline-formaldehyde photometric method [42], voltammetry [27,12], suppressed ion chromatography [35], Flow Injection Analysis (FIA) [9], Membrane Less Vaporization Unit (MBL-VP unit) using a Paired Emitter-detector Diodes and (PEDD), Coupled Contactless Detector (C4D) [15], microanalytical flow system with gas-diffusion membrane and pH ion-sensitive field effect transistor [8], and Surface-Enhanced Raman Spectroscopy (SERS) [4,3,18]. Raman spectroscopy and, in particular SERS, has been previously applied not only for sulfites quantification but also for wine quality control [30], fermentation process monitoring [38], wines discrimination [17], chemical profiling determination [22], and mycotoxins (Ochratoxin-A) detection [24]. The exhaustive control required for the correct wine production needs many chemical analyses throughout the process. Therefore, in this context, SERS is one of the most promising techniques providing good sensitivity and specificity. Through this technique, it is possible to achieve very high sensitivities approaching the target of single-molecule detection with an enhancement factor up to 10^8 when the target molecules are in proximity or absorbed onto different morphologies of some metal surfaces, graphene or semiconductors, in which metal surfaces such as gold or silver nanoparticles (NP) [41], or nanostructured metal surfaces [16,34,33] have been extensively utilized. The signal enhancing effect produced by the plasmon-active surface has been mainly attributed to two mechanisms: the Chemical Mechanism (CM) and the Electromagnetic Mechanism (EM) [37]. The first one relies on the modifications in the electronic structure of the target molecules adsorbed on the metal surfaces. In this way, some selective Raman peaks are enhanced [2]. On the other hand, the EM is produced by the enhancement of the electromagnetic field in the proximity of the rough metallic surface, enhancing both incident and scattered lights by many orders of magnitude [26]. The most widely used SERS platforms are aggregates of Au and Ag NPs induced by metal salts (Cl^-, SO_4^{2-}, and NO_3^-). Even though, the difficult reproducibility of SERS can be a drawback for quantification purposes, different approaches have been developed to ensure the reproducibility based on different NP shapes, chemical functionalization of the NPs, microfluidic devices, or the fabrication of SERS substrates among others [28,40,36]. Herein, a commercial Au nano/sub-microstructured substrate has been employed to ensure the reproducibility and easiness of use. Unfortunately, SERS has not been widely applied as a laboratory routine quantitative technique because of reproducibility problems, particularly when colloids are used as substrate, in which lack of reproducibility is associated with the final shape, size and distribution of the metal clusters generated during colloid aggregation [29,25].

Currently, under the premise of Industry 4.0 and the emergence of Internet of Things (IoT) a reliable sulfite monitoring method must fulfill the following requirements: (i) it should be accurate, (ii) simple to use (without any kind of pre-treatment), (iii) cost-effective, and (iv) suitable for in-field measurements in such way that the device could deliver the results to a web data management platform. The technological advances related to SERS tools in recent years have led to the development of affordable portable SERS devices and the commercialization of SERS substrates that avoid the time-consuming synthesis process of free NPs or NPs-coated substrates, thus enhancing the reproducibility of the method. Considering these advances, SERS is postulated as a promising technology for real-time wine quality and safety monitoring fulfilling the previously defined requirements.

The main goal of this work is to carry out a feasibility study of a new methodology for free SO_2 content monitoring based on SERS spectroscopy with the use of a laboratory Raman spectrophotometer. This work includes (i) a theoretical study based on a first-principles calculation of the Raman signal to identify the most active Raman vibrational modes of each equilibrium species that constitute free SO_2 at different pH; (ii) the development of a laboratory measurement protocol for SERS characterization considering technical requirements to transfer the methodology to a portable SERS detection module for on-site applications; and (iii) a multivariate calibration procedure for sulfites-free quantification bearing in mind the results obtained from the theoretical identification of the relevant molecular vibrational fingerprints. This methodology should be further expanded to spiked wine samples and real wine samples to check its suitability for in-field real scenarios environments.

2. Materials and methods

2.1. Raman spectrophotometer

All the SERS spectra were collected with a Renishaw (Gloucestershire, UK) in Via confocal Raman Microscope equipped with a near-infrared excitation laser of 785 nm and maximum power of 180 mW in the sample. The Raman microscope is designed to collect the back-scattered signal employing a 1200 lines/mm grating and a charge-coupled device (CCD) detector. Besides, a wide variety of different objectives from Leica (Wetzlar, Germany) is mounted on the microscope.

SERS measurements were carried out using the J12853 Au nano/sub-microstructured substrates from Hamamatsu (Shizuoka, Japan) to

ensure reproducibility and an easy manipulation of the samples. The substrates comprised nanoimprinted polypropylene coated with a thin gold film. According to the manufacturers, these substrates contain a well-established structure to facilitate attaching the solution and no sample preprocessing is required. In addition, due to the Au nanostructure, the Raman excitation wavelength used is 785 nm.

2.2. Free SO_2 aqueous solutions

As shown in Equation (1), sulfur (IV) oxoanions and sulfur dioxide in aqueous solution experiment a pH-dependent equilibrium reaction in which the following chemical species are involved: sulfur dioxide (SO_2), sulfurous acid (H_2SO_3), bisulfite ion (HSO_3^-) and sulfite ion (SO_3^{2-}). The concentration of each species depends on the pH of the medium, and it is defined by the equilibrium constants K_1 ($1{,}6 \times 10^{-2}$ mol dm^{-3}) and K_2 ($1{,}0 \times 10^{-7}$ mol dm^{-3}) [14]. At the usual pH of wine (2.8–4.0), the major specie present in the medium would be the bisulfite ion.

$$SO_2 + H_20 \overset{K_1}{\longleftrightarrow} HSO_3^- + H_30^+ \overset{K_2}{\longleftrightarrow} SO_3^{2-} + 2H_30^+ \quad (1)$$

A multivariate calibration process was performed to relate the concentration of the different species in the equilibrium reaction with the complex structure of Raman peaks obtained in SERS spectra. To that end, the following aqueous solutions of potassium metabisulfite ($K_2S_2O_5$) > 98% (Sigma Aldrich) were prepared at pH 3 and pH 6: 5 mg/l, 25 mg/l, 50 mg/l, 75 mg/l, 100 mg/l, 150 mg/l and 250 mg/l. The samples at pH 6 are those obtained directly by dissolving potassium metabisulfite in distilled water (Milli-Q). Samples at pH 3 were obtained from samples at pH 6 by adding chlorohydric acid 37% reagent grade (Scharlau) until obtaining the desired pH. Potassium disulfide in aqueous solution undergoes the reaction in Equation (2), so the ratio of potassium metabilsulfite to sulfite ion is 1:2.

$$K_2S_2O_5 + H_2O \rightarrow 2K^+ + 2SO_3^{-2} + 2H^+ \quad (2)$$

Therefore, the calibration range for free SO_2 monitoring will be defined between 10 and 500 ppm. As a simple aqueous solution is considered, it is assumed that there is no combined SO_2 and all the added metabisulfite is as free SO_2. According to Equation (1), depending on the pH of the aqueous solution, the concentration of the species that contribute to free SO_2 changes.

2.3. Raman theoretical study

The simulated Raman spectra of the molecules SO_2, SO_3^{-2}, and HSO_3^- can be obtained from Density Functional Theory (DFT) calculations of their key vibrational properties: vibrational frequencies, vibrational populations, and Raman tensors. For HSO_3^- the two existing isomers in solution were considered: one with the hydrogen atom bonded to one oxygen atom referred to as $HOSO_2^-$, and another one with the hydrogen atom bonded to the sulfur atom referred to as HSO_3^-. Based on these calculated quantities, one can obtain the total differential Stokes Raman scattering cross section for a scattering angle perpendicular to the incident light beam and the incident polarization. For a given vibrational mode k with frequency ω_k, the total differential Stokes Raman scattering cross section $\left(\frac{d\sigma}{d\Omega}\right)$ is given by [19]

$$\left(\frac{d\sigma}{d\Omega}\right) = \frac{(\omega_L - \omega_k)^4}{1440\pi^2\varepsilon_0^2 c^4 \omega_k}\left(\bar{\alpha}_k^2 + \bar{\gamma}_k^2\right)\left(1 + n_k^B(T)\right) \quad (3)$$

where ω_L is the frequency of the excitation light, $\bar{\alpha}_k^2$ and $\bar{\gamma}_k^2$ are the isotropic and anisotropic invariants of the Raman tensor of the vibrational mode k, respectively, and $n_k^B(T)$ is the thermal population of the vibrational mode k at temperature T. ε_o is the permittivity of vacuum and c is the speed of light in vacuum. In this work, we use a temperature of 298 K and an excitation light of wavelength 785 nm.

In order to simulate the chemical environment of SO_2, SO_3^{2-}, $HOSO_2^-$ and HSO_3^- in the SERS experiment, we compute the Raman spectrum of the complexes formed by these molecules bound to a tetrahedral gold cluster of 20 atoms. This chemical model configuration accounts for the contribution of the chemical mechanism to the enhancement of the molecular Raman signal observed in the SERS experiment. In addition, water molecules are explicitly included in the simulations to account for the effects of the solvent on the Raman spectra: 6 water molecules for the SO_2-Au_{20} and 8 water molecules for $SO_3^{2-}Au_{20}$, $HOSO_2^-$-Au_{20} and HSO_3^--Au_{20}. These models are referred as X-Au_{20}, with X = SO_2 $(H_2O)_6$, SO_3^{2-} $(H_2O)_8$, $HOSO_2^-$ $(H_2O)_8$ and HSO_3^- $(H_2O)_8$.

The same tetrahedral gold cluster was used, Au_{20}, optimized at the DFT level using the exchange–correlation functional B3P86 and the LANL2DZ basis set [6] for all the complexes. On top of this gold cluster structure, we add the sulfur-based compounds and the water molecules and carry out a constrained optimization of the X-Au_{20} complexes freezing the atomic positions of the gold atoms and solely allowing the atomic positions of X to relax. The B3LYP exchange–correlation functional [1] was applied to optimize the X-Au_{20} complexes. To account for the noncovalent interactions between the molecules and the gold cluster, we add the empirical dispersion D3 of Grimme [10] with the damping function of Becke and Johnson [11]. The basis set 6-311G++(d,p) was applied to characterize sulfur, oxygen and hydrogen atoms, and for the gold atoms the LANL2DZ was used as a basis set. The vibrational frequencies and Raman tensors were computed using the same exchange–correlation functional and basis sets. Vibrational frequency analysis does not reveal any imaginary frequency confirming that all structures corresponded to situations of energy minima. All calculations presented in this work were carried out with the code Gaussian 16 Rev B.01 (Gaussian 16, Revision B.01. Gaussian, Inc., Wallingford CT).

2.4. SERS characterization

According to the SERS substrate manufacturer's instructions, 5 μl of the solution was dropped in the active area of the substrates and the laser beam was focused to the center before spectra collection. The previously calibrated equipment was set to launch 80 mW of power (50 % of the maximum power) for 10 s of acquisition time. A 5X objective with a 0.12NA was employed to focus the sample. The spectra were recorded from 100 cm^{-1} to 3200 cm^{-1}. Every measurement was replicated three times.

2.5. Multivariate data analysis

Multivariate data analysis was applied to correlate the information of the vibrational fingerprints from particular spectral ranges in the SERS spectra with the free SO_2 concentration of $K_2S_2O_5$ aqueous solutions at pH 3 and 6. To optimize the spectroscopic information, different types of pre-processing methods and combinations were applied to the spectra such as baseline removal, Moving Average and Savitzky-Golay (SG) smoothing, Multivariate Scatter Correction (MSC), Standard Normal Variate (SNV) or derivatives. Once the pre-processing strategy was defined, the next step was the development of the calibration model. The mathematical model was developed by Partial Least Square Regression (PLSR). This regression technique has been previously applied by other authors for wine quality monitoring in Raman/SERS spectroscopy [38,30,5,41]. Then, the Martens Uncertainty test for variable selection was applied to the mathematical model. This is a cost-effective method proposed by Westad & Martens, that applies the principle of Jack-Knifing for estimating standard errors of the regression coefficients in the PLSR [39]. This method gives good results with a reduced number of samples, compared to other variable selection methods such as an interval Partial Least Square Regression (iPLS) or Genetic Algorithms (GAs) that work better with more samples [31,32]. By application of the Martens test, regression coefficients of the mathematical model are divided by their estimated standard errors to give test-t values for testing

the significance of the variables used in the model. The PLSR model was then redone using only the spectroscopic variables selected by the Martens test. Considering the limited number of available samples, the validation of the models was carried out by the leave-one cross-validation method. The calibration model performance was assessed according to the statistical parameters obtained from the validation such as the coefficient of determination (r^2), Root Mean Square Error of Cross Validation (RMSECV), Standard Error of Cross Validation (SECV) and Bias. The optimum number of Latent Variables (LVs) of the model was selected considering the variation of RMSECV with the number of LVs.

The data analysis was carried out with The Unscrambler X ver. 10.5 software (CAMO Software AS, Oslo, Norway) and with a script developed in the R software implemented in the hyperSpec package.

3. Results and discussion

3.1. Identification of the target Raman peaks

To identify the most representative Raman lines of all the chemical species that contribute to the total concentration of free SO_2 (Eq. (1)–(2)) in the SERS measurements in water, the Raman spectra of the complexes X-Au_{20} is calculated, Fig. 1. From these spectra the wavenumbers of the stretching and bending vibrational modes of the selected molecules are identified, namely SO_2, SO_3^{2-}, $HOSO_2^-$, and HSO_3^- in the complexes X-Au_{20} as shown in Table 1. For the sake of simplicity, the wavenumbers of the bending modes of the water molecules that appear between 1615 cm^{-1} and 1743 cm^{-1} in all the studied complexes are omitted.

In the spectra of SO_2 $(H_2O)_6$-Au_{20} and SO_3^{2-} $(H_2O)_8$-Au_{20} (Fig. 1a and Fig. 1b and Table 1) it is observed a number of Raman lines between 465 cm^{-1} and 612 cm^{-1} corresponding to the O—S—O bending modes, and a group of lines at higher wavenumbers ranging from 917 cm^{-1} to 1278 cm^{-1}, corresponding to the S—O stretching modes. The two spectra are dominated by the Raman lines of the S—O symmetric stretching mode at 1145 cm^{-1} for SO_2 $(H_2O)_6$-Au_{20} and at 918 cm^{-1} for SO_3^{2-} $(H_2O)_8$-Au_{20}, which are selectively enhanced as compared to the same Raman lines of the molecules without the gold cluster. For SO_2-Au_{20} the Raman line of the S-O symmetric stretching is enhanced by a factor of 10 (compare relative strengths in Fig. S1a and Fig. S1e) due to the interaction of the molecules with the gold cluster. For SO_3^{2-}-Au_{20} the resonances of the cluster enhance the Raman line of the S-O symmetric stretching almost by a factor 10^7 (compare Fig. S1b and Fig. S1f). Thus, it is expected that the position of the Raman lines of this mode changes rapidly with the pH of the sample. For HSO_3^- $(H_2O)_8$-Au_{20} (Fig. 1d). It is noticed that the interaction of HSO_3^- with the gold cluster almost exclusively enhances the Raman line of the S-H stretching mode at 2378 cm^{-1}, that is one order of magnitude more intense than the rest of the modes of the molecule (compare Fig. S1d with Fig. S1h).

The theoretical analysis of the Raman spectra of the complexes X-Au_{20}, reveals that the most prominent features for the determination of all the chemical species that contribute to the total concentration of SO_2 are the Raman lines of the S—O stretching modes, the O—H stretching modes of $HOSO_2^-$ and the S—H stretching mode of HSO_3^-. In order to correlate the concentration of SO_2, SO_3^{2-}, HSO_3^- with the intensity of the

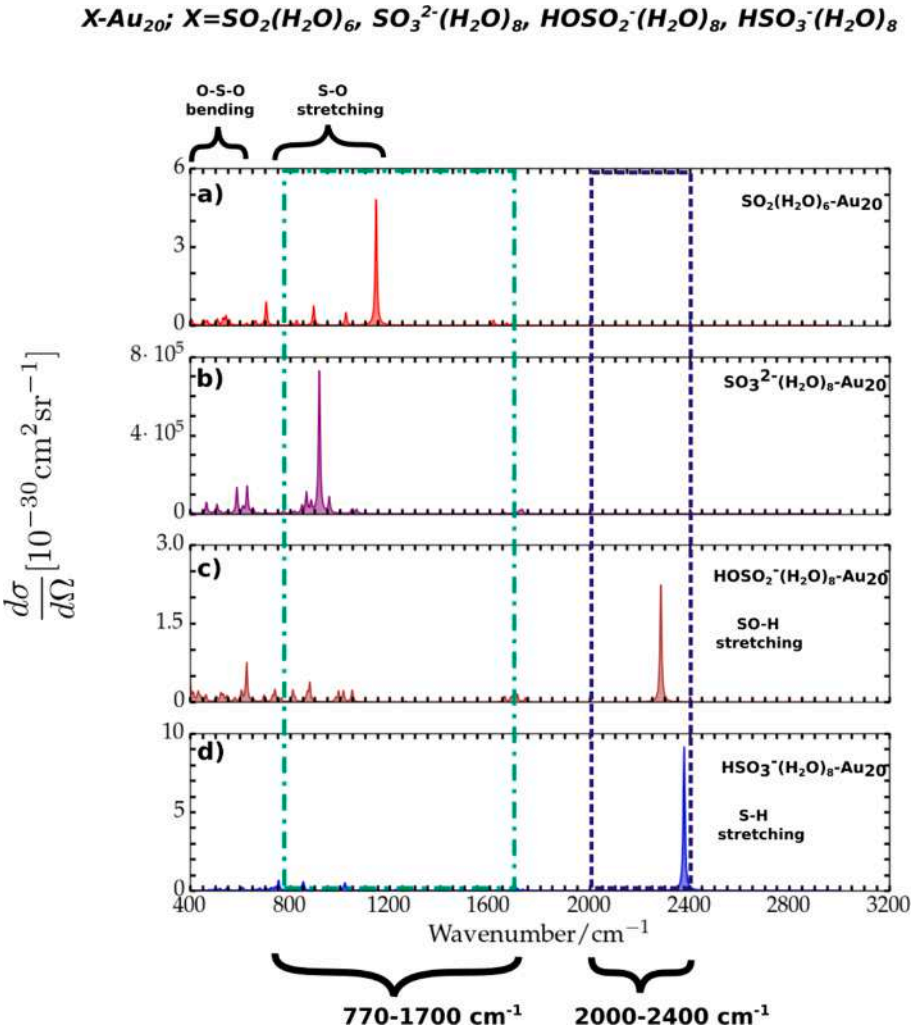

Fig. 1. Simulated Raman spectra of SO_2 $(H_2O)_6$-Au_{20}, SO_3^{2-} $(H_2O)_8$-Au_{20}, $HOSO_2^-$ $(H_2O)_8$-Au_{20} and HSO_3^- $(H_2O)_8$-Au_{20}. The Raman absolute differential cross-section $\left(\frac{d\sigma}{d\Omega}\right)$ as a function of the wave number between 400 cm^{-1} and 3200 cm^{-1} calculated at B3LYP-D3(BJ)/6-311G++(d,p)/LANL2DZ level. a) Raman spectrum of SO_2 $(H_2O)_6$-Au_{20}; b) SO_3^{2-} $(H_2O)_8$-Au_{20}; c) $HOSO_2^-$ $(H_2O)_8$-Au_{20}, and d) HSO_3^- $(H_2O)_8$-Au_{20}. The green and blue dashed lines highlight the spectroscopy working ranges 770–1700 cm^{-1} and 2000–2400 cm^{-1}, respectively.

Table 1
Calculated vibrational wavenumber of SO_2 $(H_2O)_6$-Au_{20}, SO_3^{2-} $(H_2O)_8$-Au_{20}, $HOSO_2^-$ $(H_2O)_8$ $^-Au_{20}$ and HSO_3^- $(H_2O)_8$-Au_{20}. The vibrational frequencies at B3LYP-D3 (BJ)/6-311G++(d, p)/LANL2DZ level were computed. First column: Chemical formula of the studied complexes. Second column: assignment of the vibrational modes where ν_s, ν_a and δ stand for the symmetric (Sym.) stretching, asymmetric (Asym.) stretching and bending modes, respectively. Third column: Description of the vibrational modes. Fourth column: Calculated wavenumbers in cm^{-1}. The vibrational modes within the spectroscopic ranges used to develop the multivariate model in section 4.2 are highlighted. The rows colored in green, and blue contain the vibrational modes in the spectroscopic ranges from 770 cm^{-1} to 1400 cm^{-1}, and from 2000 cm^{-1} to 2400^{-1} respectively.

Complex	Assignment	Description	Wavenumber (cm^{-1})
SO_2 $(H_2O)_6$-Au_{20}	$\nu_a(S-O)$	Asym. stretching	1278.45
	$\nu_s(S-O)$ $\delta(S-O)$	Sym. stretching	1145.12
		Bending	532.40
SO_3^{2-} $(H_2O)_8$ - Au_{20}	$\nu_a(S-O)$ $\nu_a(S-O)$	Asym. stretching	1048.13
	$\nu_s(S-O)$ $\delta(S-O)$	Asym. stretching	976.13
	$\delta(S-O)$	Sym. stretching	917.83
	$\delta(S-O)$	Bending	611.90
		Bending	493.43
		Bending	465.77
$HOSO_2^-$ $(H_2O)_8$ - Au_{20}	$\nu(O-H)$ $\nu_a(S-O)$	Stretching	2258.18
	$\nu_s(S-O)$ $\nu_s(S-O)$ $\delta(S-O)$	Asym. stretching	1014.46
	$\delta(S-O)$ $\delta(S-O)$	Sym. stretching	982.62
	$\delta(S-O)$	Sym. stretching	820.31
		Bending	579.06
		Bending	463.79
		Bending	440.41
		Bending	432.34
HSO_3^- $(H_2O)_8$ - Au_{20}	$\nu(S-H)$ $\nu_a(S-O)$	Stretching	2378.45
	$\nu_a(S-O)$ $\delta(S-O)$ $\delta(S-O)$	Asym. stretching	1223.31
	$\nu_s(S-O)$ $\delta(S-O)$	Asym. stretching	1194.63
	$\delta(S-O)$ $\delta(S-O)$	Bending	1125.05
	$\delta(S-O)$	Bending	1107.05
		Sym. stretching	1020.53
		Bending	605.39
		Bending	490.11
		Bending	477.59

spectral fingerprints in the SERS measurements, there are developed in the following section a multivariate model selecting specific spectroscopic ranges, where it is adopted the following criteria: i) the spectral range must include the relevant Raman fingerprints of the analyzed molecules as revealed by the simulated spectra; ii) the spectral range must expand over a narrow wavenumber window to keep the level of noise of the multivariate model to a minimum. By following these criteria, two spectroscopic ranges are selected: one from 770 cm^{-1} to 1700 cm^{-1} that includes the S—O stretching modes (Table 1 green rows; Fig. 1 region between the green dashed lines), and other from 2000 cm^{-1} to 2400 cm^{-1} that includes the O—H and S—H stretching modes (Table 1 blue rows; Fig. 1 region between the blue dashed lines).

3.2. Optimization of calibration model performance

The first step in the processing of the experimental SERS spectra was to attenuate/ remove the undesirable baseline effect employing 4S Peak filling Algorithm (hyperSpec package). According to the results obtained in Section 3.1, the spectroscopic working range of 770–1700 cm^{-1} + 2000–2400 cm^{-1} was selected. The most appropriate mathematical preprocessing strategy was then defined, which consisted of (1) smoothing Savitzky-Golay (size = 11, polynomial order = 2) to remove the spectroscopic noise of the experimental data; (2) SNV to correct multiplicative effects of spectra, and finally (3) centering of all spectra. Fig. 2a and Fig. 2b show representative raw SERS spectra at pH 3 and pH 6 respectively and, Fig. 3a and Fig. 3b show SERS spectra after applying

the chosen pre-processing strategy (Fig. S3a/S3b and Fig. S3c/S3d shows the spectra obtained after baseline removal and smoothing by Savitzky-Golay process at pH3 and pH6 respectively). The most significative changes between them are due to the application of SNV. The main effect of SNV is to center the data at the average level of the spectrum and scale the data to unit variance [44]. Basically, the resulting processed spectrum appears centered at zero and shows a variation of approximately −2 to +2 on the vertical scale.

Considering the number of available samples, the validation of the calibration models was carried out by leave-one-out cross-validation. Table 2 shows the performance of the multivariate calibration models with and without the Martens Uncertainty test variable selection method at pH 3 and pH 6. Results show how the main statistics related to the model's performance have been improved by the Martens test: r^2 increase from 0.757 to 0.904 at pH 3, and from 0.842 to 0.915 at pH 6. SECV decreases from 82.02 to 51.50 at pH 3 and from 66.44 to 47.71 at pH 6 reducing the prediction error of the models, and the number of LVs drops from 4 to 3 at pH 3 and from 4 to 2 at pH 6. With the use of this method, it has been possible to remove non-informative variables decreasing the error of the model and improving its robustness with a smaller number of LVs. Fig. 4a and Fig. 4b show the correlation between the predicted and the reference values of free SO_2 of the models obtained after applying Martens test at pH 3 and 6, including a description of all statistics obtained after cross-validation and the number of LVs (factors) used in the model. Fig. 5a and Fig. 5b show the variation of RMSECV with the number of LVs (factors) at pH 3 and 6, where the minimum

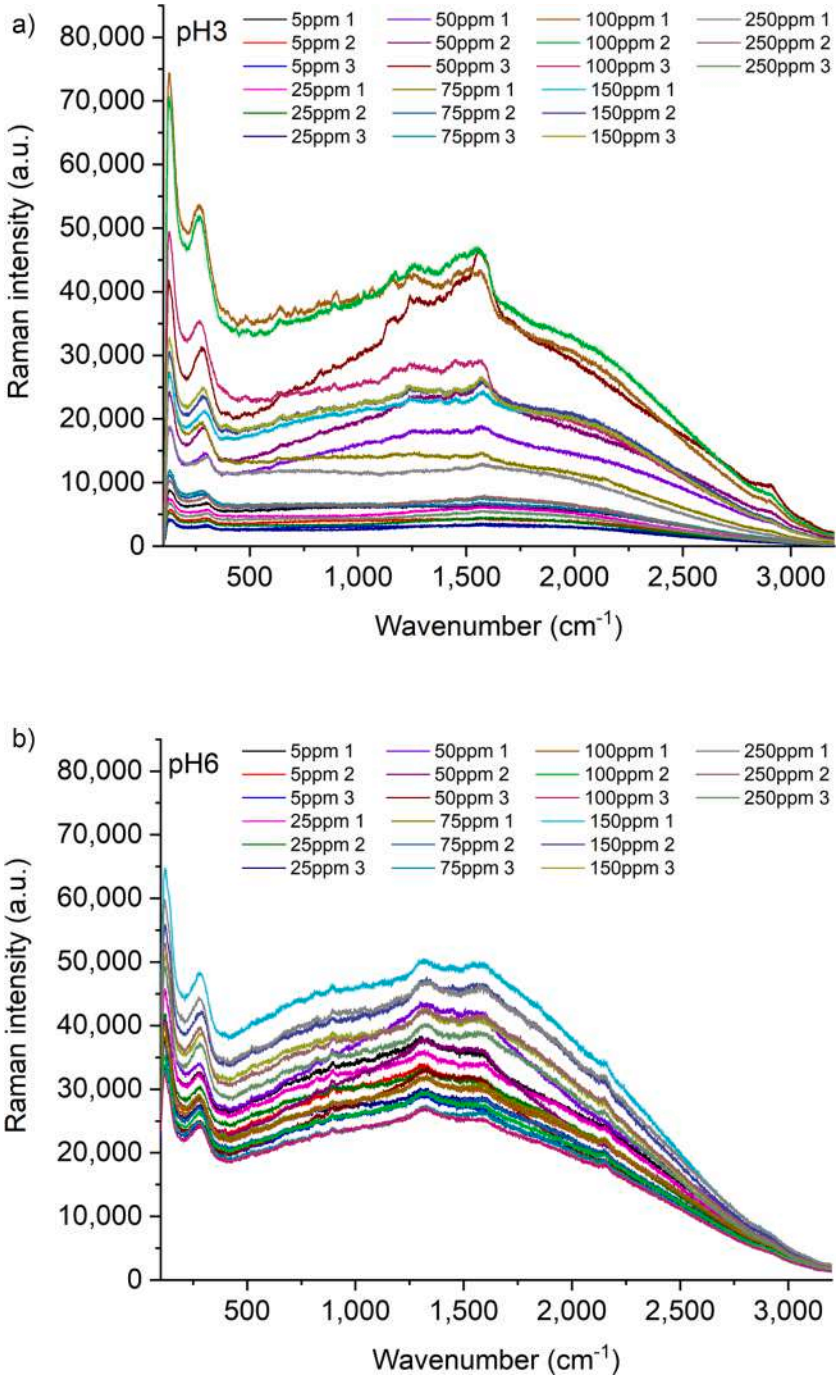

Fig. 2. Raw SERS spectra at pH 3 (a) and pH 6 (b).

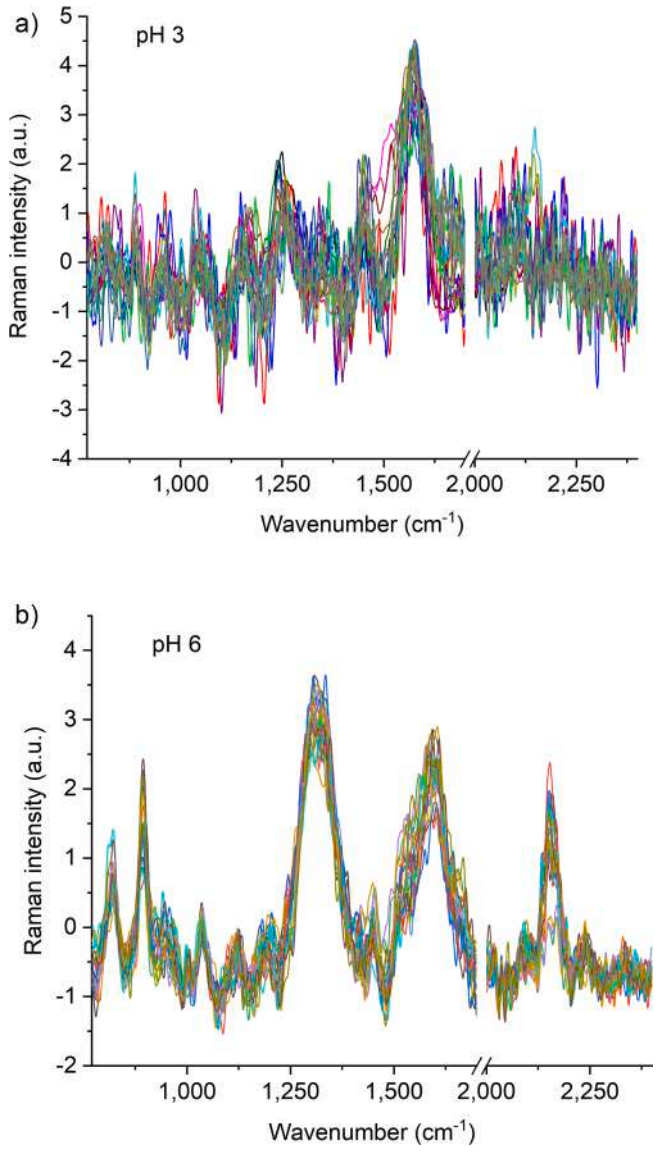

Fig. 3. SERS spectra at pH3 (a) and pH6 (b) after pre-processing process (smoothing Savitzky Golay + SNV + centering).

value of RMSECV, hence the optimum number of LVs of multivariate models, corresponds to 3 and 2, respectively. Results show how the combination of the selected spectral range obtained from theoretical calculations with the variable selection guided by the Martens tests provides a good approach, pointing out the potential of the model to predict the concentration of free SO2 in certain samples of wine.

Fig. 6a and Fig. 6b show the most significant regression coefficients (highlighted in red) calculated by Martens test at pH 3 and 6 respectively. As expected, the results obtained are not the same, because the concentration of the chemical species that contribute to free SO_2 varies as a function of pH. According to these results, Table 3 shows the most significant variables selection (Raman peaks) done by the Martens test at pH 3 and pH 6. At pH 6 the main species in equilibrium would be HSO_3^- and SO_3^{2-}, with a residual contribution of SO_2. Therefore, it is expected that the selected variables will be related to the above-mentioned compounds. Taking as a reference the theoretical study described in Section 3.1, it is described that bands between 1048.72 and 1047.77 cm^{-1} and 973.06–968.09 cm^{-1} could be linked with the asymmetric stretching modes of SO_3^{2-}. Likewise, bands at 2365.81–2350.45 cm^{-1} can be associated with the stretching mode (S—H) of HSO_3^-, and bands between 1242.89 and 1217.17 cm^{-1} and 1164.41–1155.09 cm^{-1} could be linked with the asymmetric stretching mode (S—O) of HSO_3^-. In addition, bands between 2255.63 and 2251.13 cm^{-1} can be related to the stretching mode (O—H) of $HOSO_2^-$ and bands between 989.06 and 983.66 cm^{-1} 800.60–799.60 cm^{-1} would correspond to the symmetric stretching (S—O) of $HOSO_2^-$.

Following the same approach, at pH 3 the main species in equilibrium would be SO_2 and HSO_3^-. Thus, it is expected that selected variables will be related to them. Once again, taking as a reference the theoretical study, it is described that the bands between 1275.12 and 1236.53 could be assigned to the asymmetric stretching mode of SO_2. Similarly, the bands between 2259.27 and 2258.53 cm^{-1} and 1225.45–1210.64 cm^{-1} are probably related to the stretching mode (O—H) of $HOSO_2^-$ and asymmetric stretching mode (S—O) of HSO_3^-, respectively.

Finally, relevant bands associated with active vibration modes of water are observed in the calibration models. At pH 6 the bands between 1700.22 and 1696.03 cm^{-1}, 1693.51–1681.76 cm^{-1}, and 1669.14–1644-64 cm^{-1} could be assigned to the bending mode (H—O—H) of H_2O in: SO_3^{2-} $(H_2O)_8$-Au_{20}, HSO_3^- $(H_2O)_8$-Au_{20} and $HOSO_2^-$ $(H_2O)_8$-Au_{20}. Likewise, at pH 3 the bands between 1694.05 and 1683.93 cm^{-1}, 1672.95–1671.25 cm^{-1}, 1661.08–1657.69 cm^{-1}, 1645.79–1636.43 cm^{-1}, and 1621.06–1617.64 cm^{-1} could be assigned to the bending mode (H—O—H) of H_2O in: SO_2 $(H_2O)_6$-Au_{20}, HSO_3^- $(H_2O)_8$-Au_{20} and $HOSO_2^-$ $(H_2O)_8$-Au_{20}.

In summary, the theoretical calculations carried out to identify the Raman active vibrations of the different molecules involved in the chemical equilibrium of free SO_2 in an aqueous solution provides an excellent input for the selection of variables for multivariate data analysis. This selection of spectral bands can be additionally improved by means of a Martens test, which provides a more robust output in terms of selected spectral ranges contributing to the prediction model.

4. Conclusions

The results obtained in this work show the feasibility to monitor the free SO_2 content in aqueous solution at different pH by the SERS methodology described here. The protocol followed in this work integrates the theoretical study reflecting the Raman active vibrations of molecules alongside their expected frequencies and contribution to the Raman signal with a multivariate data analysis that takes this theoretical information as an input for initial variables selection. The described route should be the basic step for sensing-based applications, more specifically for those based on Raman scattering or infrared absorption spectroscopies in which the target molecules have well defined fingerprints associated with their environment, symmetry, and vibrational selection rules. Thus, multivariate data analysis, required to handle the complex spectra information, works from the solid base of knowledge

Table 2
Performance of the multivariate calibration models with and without the Martens Uncertainty test at pH 3 and 6.

pH	Variable Selection	r^2	RMSECV	SECV	Bias	LVs
3	Theoretical (Section 4.1)	0.757	80.627	82.020	9.677	4
	Theoretical + Martens test	0.904	50.509	51.503	4.988	3
6	Theoretical (Section 4.1)	0.842	64.956	66.445	−3.820	4
	Theoretical + Martens test	0.915	47.566	48.714	−1.546	2

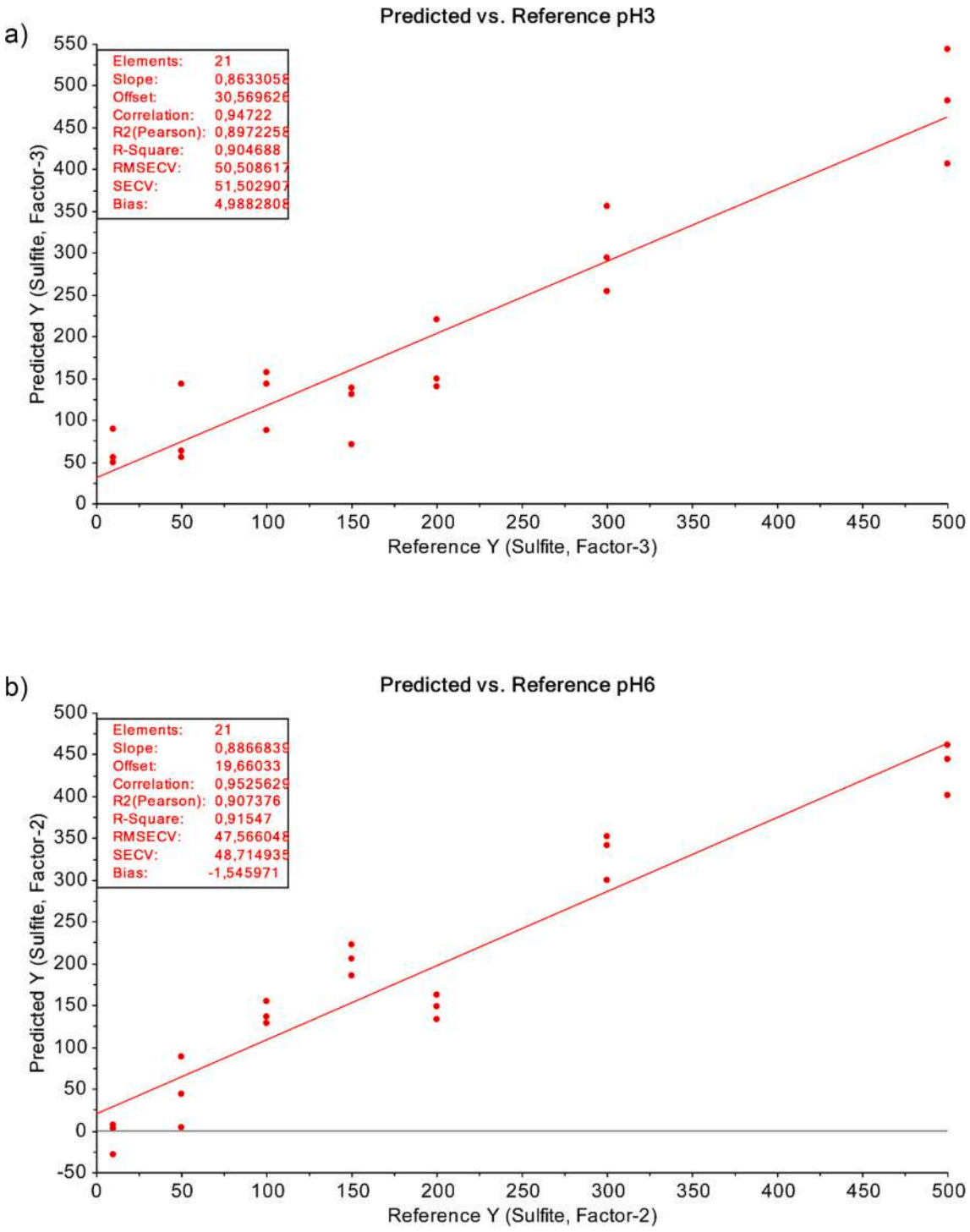

Fig. 4. Correlation between the reference values (concentration of free SO_2 determined in Section 2.2) and the predicted values obtained by Martens tests calibration models at pH 3 (a) and pH 6 (b) with the main statistics calculated after cross-validation and the number of LVs (factor) used in the model.

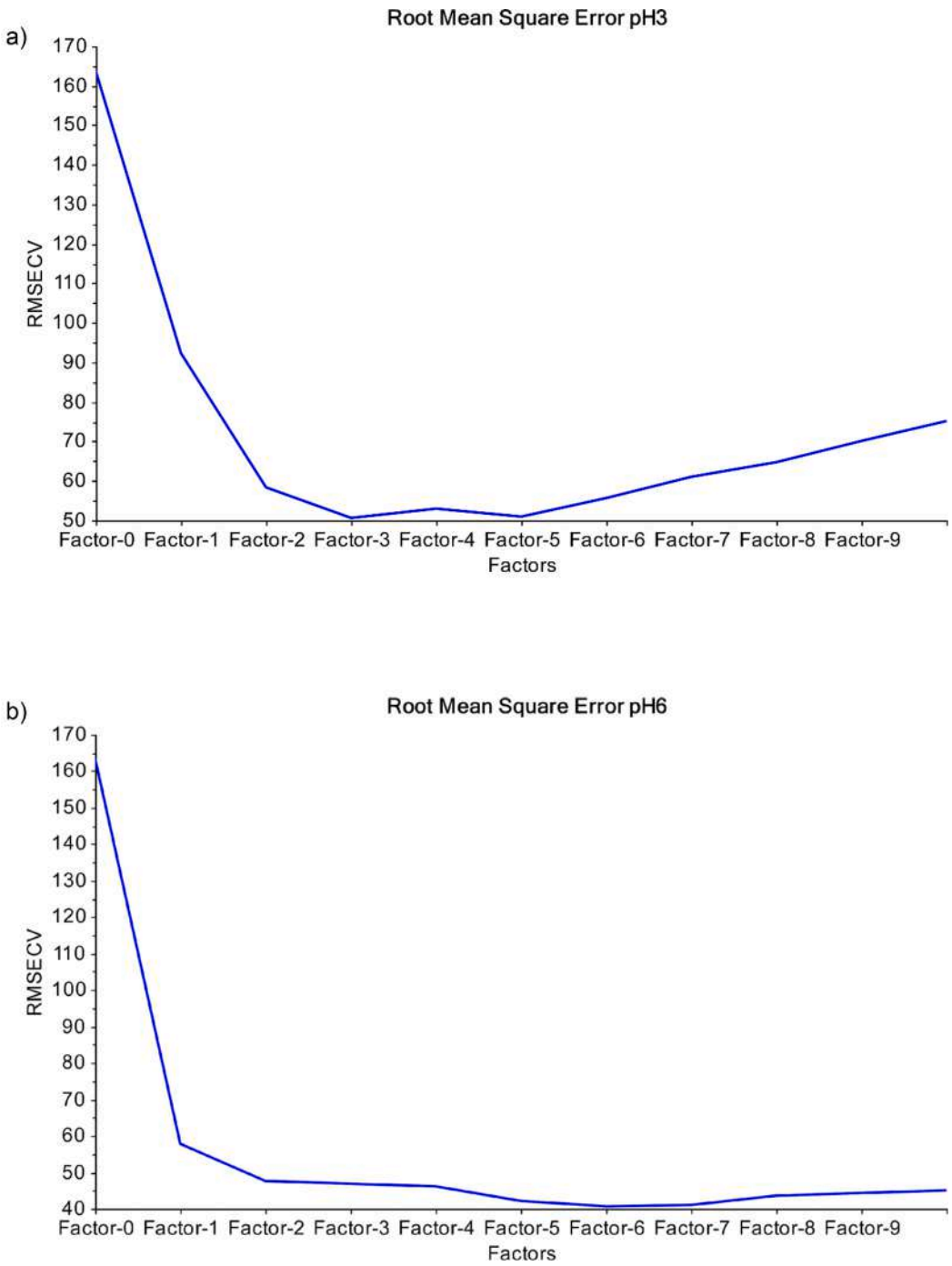

Fig. 5. Variation of RMSECV with the number of LVs (factors) at pH 3 (a) and pH 6 (b), showing the optimal number of LVs for each of the calibration models (3 and 2, respectively).

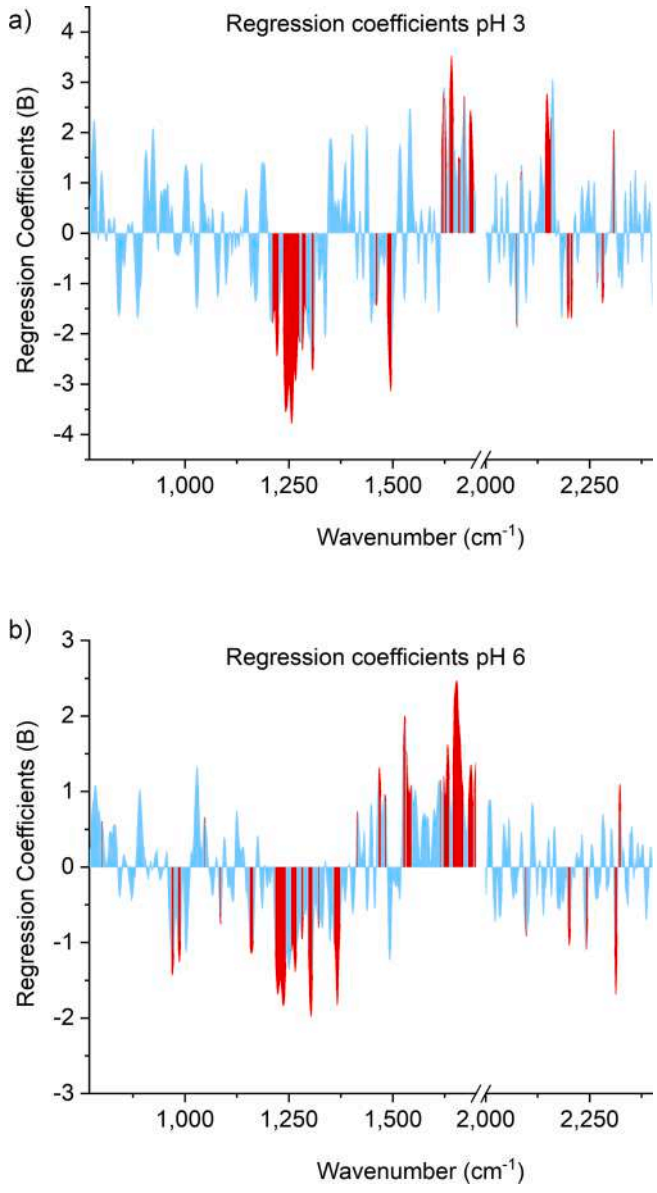

Fig. 6. The most significant regression coefficients (B) highlighted in red of the calibration models determined by the Martens Uncertainty tests at pH 3 (a) and pH 6 (b).

enhancing the output model.

Although this methodology must be optimized to improve aspects such as the prediction error, it can be a useful tool for on-site monitoring in industrial applications, where for a rapid diagnostic a semi-quantitative technique can be very helpful. In this context, the aim of developing SERS methodology is not to reach the accuracy and precision features of Moinier-Williams or Ripper standard methods but to offer the possibility of a rapid and easy method that allows for monitoring for fast corrective actions. This methodology has been conceived to be used by nonspecialized personnel, not requiring any complex sample pre-processing, just take out an aliquot of the sample, deposit it on the SERS substrate and measure. The reproducibility problems associated with SERS technique are mitigated using commercial SERS substrates, avoiding the synthesis of AuNPs colloids. Regarding the equipment costs, nowadays there are on the market cost-effective portable Raman spectrophotometers with acceptable performance that can be used for this type of applications. The future trend of Raman/SERS technology is that the equipment manufacturing cost will decrease as technological advances progress, providing a lower retail price, making their implementation in the industry increasingly attractive.

Future work should be focused on transferring the methodology to portable Raman devices and performing a multivariate calibration with wine samples. Whilst 97% of the liquid in wine is water and ethanol, the remaining 3% contains hundreds of discrete molecules from acids and sugars to aroma and phenolic compounds. It constitutes a quite heterogeneous composition which could probably provide a strong spectral interference. It would need an exigent calibration process in which the optimal bands for sulfite detection may be modified. During the calibration process, it would be necessary to characterize as many samples as possible, which would allow not only to obtain a more robust calibration model, but also to perform a more representative validation with a prediction test set. Similarly, by characterizing more wine samples, it would be possible to use other more powerful variable selection methods (e.g., iPLS or GA), which will allow us to obtain better calibration results.

5. Author statement

Alberto Villar: Methodology, Data Curation, Investigation, Writing – original draft.

Santos Merino: SERS methodology, Conceptualization, Investigation, Supervision.

Roberto A. Boto: Density Functional Theory calculations of the Raman spectra and interpretation of the theoretical results.

Javier Aizpurua: Design, coordination and interpretation of the theoretical results of the Raman peaks.

Aitzol Garcia: Input on theoretical interpretation of the Raman lines.

Mikel Azkune: SERS methodology and characterization**,** Multivariate Data Analysis.

Joseba Zubia: Conceptualization, Investigation, Supervision.

CRediT authorship contribution statement

Alberto Villar: Methodology, Data curation, Investigation, Writing – original draft. **Santos Merino:** Methodology, Conceptualization, Investigation, Supervision. **Roberto A. Boto:** . **Javier Aizpurua:** . **Aitzol Garcia:** . **Mikel Azkune:** Methodology, Data curation. **Joseba Zubia:** Conceptualization, Investigation, Supervision.

Table 3
The most significant spectroscopic variables determined by the Martens Uncertainty tests. Variables in bold coincide with those determined through the theoretical study in Section 3.1.

Parameter	Most Significant Variables (cm^{-1})
SO_2 free at pH 3	2283.98–2279.52, **2259.27–2258.53**, 2230.86, 2208.22–2204.44, 2201.41–2196.11, 2157.27–2143.48, 2084.82–2084.04, 2074.71–2073.93, 1694.05–1683.93, 1672.95–1671.25, 1661.08–1657.69, 1645.79–1636.43, 1629.60–1625.33, 1621.06–1617.64, 1497.26–1486.73, 1462.96–1459.43, 1310.70–1305.24, 1290.66–1281.52, **1275.12–1236.53, 1225.45–1210.64**.
SO_2 free at pH 6	**2365.81–2350.45**, 2315.50–2310.35, **2255.63–2251.13**, 2203.86–2198.58, 2097.93–2095.61, 1700.22–1696.03, 1693.51–1681.76, 1669.14–1644-64, 1636.16–1622-57, 1614.91–1614.06, 1545.42–1525.52, 1483.71–1481.09, 1471.46–1466.32, 1415.04–1413.27, 1373.21–1358.89, 1322.02–1320.21, 1306.65–1296.78, 1284.88–1279.42, 1268.49–1254.71, **1242.89–1217.17**, **1164.41–1155.09**, 1086.62–1083.78, **1048.72–1047.77**, **989.43–983.66**, **973.06–968.24**, **800.60**–799.60.

Declaration of Competing Interest

The authors declare the following financial interests/personal relationships which may be considered as potential competing interests: Alberto Villar Verguizas reports financial support was provided by European Commission. Alberto Villar Verguizas reports financial support was provided by Basque Government.

Data availability

Data will be made available on request.

Acknowledgments

The authors gratefully acknowledge the collaboration of the wineries Terras Gaudas and Roda. This work has been funded in part by the Fondo Europeo de Desarrollo Regional (FEDER), in part by the Ministerio de Ciencia, Innovación y Universidades under projects PID2021-122505OB-C31, PID2019-107432GB-I00, in part by the GobiernoVasco/Eusko Jaurlaritza IT1452-22, IT1526-22, ELKARTEK KK-2021/00092 and ELKARTEK KK-2021/00082.

Appendix A. Supplementary material

Supplementary data to this article can be found online at https://doi.org/10.1016/j.saa.2023.122899.

References

[1] A.D. Becke, A new mixing of Hartree-Fock and local density-functional theories, J. Chem. Phys. 98 (1993) 1372–1377, https://doi.org/10.1063/1.464304.
[2] R. Chen, L. Jensen, Interpreting the chemical mechanism in SERS using Raman bond model, J. Chem. Phys. 152 (2020), 024126, https://doi.org/10.1063/1.5138204.
[3] M. Chen, H. Yang, L. Rong, X. Chen, A gas-difussion microfluidic paper-based analytical device (μPAD) coupled with portable surface-enhanced Raman scattering (SERS): facile determination of sulfite in wines, Analyst 141 (2016) 5511, https://doi.org/10.1039/C6AN00788K.
[4] Z. Deng, C. Xuexu, Y. Wang, E. Fang, Z. Zhang, X. Chen, Headspace thin-film microextraction coupled with surface-enhanced Raman scattering as a facile method for reproducible and specific detection of sulfur dioxide in wine, Anal. Chem. 87 (2014) 633–640, https://doi.org/10.1021/ac503341g.
[5] V. Deneva, I. Bakardzhisky, K. Bambalov, D. Antonova, D. Tsobanova, V. Bambalov, D. Cozzolino, L. Antonov, Using Raman spectroscopy as a fast tool to classify and analyze Bulgarian wines: A feasibility study, Molecules 25 (2019) 170, https://doi.org/10.3390/molecules25010170.
[6] P.J. Hay, W.R. Wadt, Ab initio effective core potentials for molecular calculations. Potentials for K to Au including the outermost core orbitals, J. Chem. Phys. 82 (1) (1985) 299–310, https://doi.org/10.1063/1.448975.
[7] A.R. Garcia-Fuentes, S. Wirtz, E. Vos, H. Verhagen, Short review of sulphites as food additives, Eur. J. Nutr. Food Saf. 5 (2015) 113–120, https://doi.org/10.9734/EJNFS/2015/11557.
[8] P. Gimenez-Gomez, M. Gutierrez-Capitán, J.M. Ríos, F. Capdevila, A. Puig-Pujol, C. Jiménez-Jorquera, Microanalytical flow system for the simultaneous determination of acetic acid free sulfur dioxide wines, Food Chem. 346 (2021), 128891, https://doi.org/10.1016/j.foodchem.2020.128891.
[9] L.M. Gonçalves, J. Grosso Pacheco, P.J. Magalhaes, J.A. Rodrigues, A. Araújo Barros, Determination of free and total sulfites in wine using an automatic flow injection analysis system with voltammetric detection, Food Addit. Contam. 27 (2009) 175–180, https://doi.org/10.1080/19440040903261547.
[10] S. Grimme, J. Antony, S. Ehrlich, H. Krieg, A consistent and accurate *ab initio* parametrization of density functional dispersion correction (DFT-D) for the 94 elements H-Pu, J. Chem. Phys. 132 (2010) 154104–1541023, https://doi.org/10.1063/1.3382344.
[11] S. Grimme, S. Ehrlich, L. Goerigk, Effect of the damping function in dispersion corrected density functional theory, J. Comput. Chem. 32 (2011) 1456–1465, https://doi.org/10.1002/jcc.21759.
[12] A. Guarda, J. Villela Maciel, B. Avila Wiethan, A. Schneider, P. Cícero do Nascimiento, D. Dias, Simultaneous determination of ethanetiol, inorganic sulfide, and sulfite in wines by cathodic stripping voltammetry, Food Anal. Methods 10 (2017) 837–844, https://doi.org/10.1007/s12161-016-0640-1.
[13] R.F. Guerrero, E. Cantos-Villar, Demonstrating the efficiency of sulphur dioxide replacements in wine: A parameter review, Trends Food Sci. Technol. 42 (2014) 27–43, https://doi.org/10.1016/j.tifs.2014.11.004.
[14] L.F. Guido, Sulfites in beer: reviewing regulation, analysis, and role, Sci. Agric. 73 (2016) 189–197, https://doi.org/10.1590/0103-9016-2015-0290.
[15] P. Kraikaew, T. Pluangklang, N. Ratanawimarnwong, K. Uraisin, P. Wilairat, T. Mantim, D. Nacapricha, Simultaneous determination of ethanol and total sulfite in white using on-line cone reservoirs menbraneless gas-liquid separation flow system, Microchem. J. 149 (2019), 104007, https://doi.org/10.1016/j.microc.2019.104007.
[16] J. Langer, D. Jimenez de Aberasturi, J. Aizpurua, R.A. Alvarez-Puebla, B. Auguié, J. J. Baumberg, G.C. Bazan, S.E.J. Bell, A. Boisen, A.G. Brolo, J. Choo, D. Cialla-May, V. Deckert, L. Fabris, K. Faulds, F.J. García de Abajo, R. Goodacre, D. Graham, A. J. Haes, C.L. Haynes, C. Huck, T. Itoh, M. Käll, J. Kneipp, N.A. Kotov, H. Kuang, E. C. Le Ru, H.K. Lee, J.-F. Li, X.Y. Ling, S.A. Maier, T. Mayerhöfer, M. Moskovits, K. Murakoshi, J.-M. Nam, S. Nie, Y. Ozaki, I. Pastoriza-Santos, J. Perez-Juste, J. Popp, A. Pucci, S. Reich, B. Ren, G.C. Schatz, T. Shegai, S. Schlücker, L.-L. Tay, K. G. Thomas, Z.-Q. Tian, R.P. Van Duyne, T. Vo-Dinh, Y. Wang, K.A. Willets, C. Xu, H. Xu, Y. Xu, Y.S. Yamamoto, B. Zhao, L.M. Liz-Marzán, Present and future of surface-enhanced Raman scattering, ACS Nano 14 (1) (2020) 28–117, https://doi.org/10.1021/acsnano.9b04224.
[17] D.A. Magdas, S.C. Pinzaru, F. Guyon, I. Feher, B.I. Cozar, Application of SERS technique in white wines discrimination, Food Control 92 (2018) 30–36, https://doi.org/10.1016/j.foodcont.2018.04.043.
[18] L. Mandrile, I. Cagnasso, L. Berta, A.M. Giovannozzi, M. Petroziello, F. Pellegrino, A. Asproudi, F. Durbiano, A.M. Rossi, Direct quantification of sulfur dioxide in wine by surface enhanced Raman spectroscopy, Food Chem. 326 (2020), 127009, https://doi.org/10.1016/j.foodchem.2020.127009.
[19] J. Neugebauer, M. Reiher, C. Kind, B.A. Hess, Quantum chemical calculation of vibrational spectra of large-Raman and IR spectra from Buckminsterfullerene, J. Comput. Chem. 23 (2002) 895–910, https://doi.org/10.1002/jcc.10089.
[21] M.A. Pazo-Bayon, M. Monagas, B. Bartolomé, M. Moreno-Arribas, Wine features related to safety and consumer health: An integrated perspective, Crit. Rev. Food Sci. Nutr. 52 (2012) 31–54, https://doi.org/10.1080/10408398.2010.489398.
[22] Y. Qu, Y. Tian, Y. Chen, L. He, Chemical profiling of red wines using surface-enhanced Raman spectroscopy (SERS), Anal. Methods 12 (2020) 1324–1332, https://doi.org/10.1039/D0AY00099J.
[23] Ribereau-Gayon, P., Dubourdieu, D., Doneche, B., & Lonvaud, A. (2006). Handbook of enology: The microbiological of wine and vinifications, Vol. 1 (2nd ed.). Chichester. Wiley.
[24] S. Rostami, K. Zór, D.M. Zhai, M. Viehrig, L. Morelli, A. Mehdinia, J. Smedsgaard, T. Rindzevicius, A. Boisen, High-throughput label-free detection of Ocharatoxin A in wine using supported liquid membrane extraction and Ag-capped silicon nanopillar SERS substrates, Food Control 113 (2020), 107183, https://doi.org/10.1016/j.foodcont.2020.107183.
[25] J.J. Santos, S.H. Toma, P. Corio, K. Araki, Key role of surface concentration on reproducibility and optimization of SERS sensitivity, J. Raman Spectrosc. 48 (2017) 1190–1195, https://doi.org/10.1002/jrs.5203.
[26] G.C. Schatz, M.A. Young, R.P. Duyne, Electromagnetic mechanism of SERS, in: Surface-Enhanced Raman Scattering, Springer, Berlin Heidelberg, 2006, pp. 19–45.
[27] E.M. Silva, R.M. Takeuchi, A.L. Santos, Carbon nanotubes for voltametric determination of sulfite in some beverages, Food Chem. 173 (2015) 763–769, https://doi.org/10.1016/j.foodchem.2014.10.106.
[28] K.R. Strehle, D. Cialla, P. Rösch, T. Henkel, M. Köhler, J. Popp, A reproducible surface-enhanced Raman spectroscopy approach. Online SERS measurements in a segmented microfluidic system, Anal. Chem. 79 (2007) 1542–1547, https://doi.org/10.1021/ac0615246.
[29] T. Rantra, R.J.C. Brown, M.J.T. Milton, Strategy to improve the reproducibility of colloidal SERS, J. Raman Spectrosc. 38 (2007) 1469–1479, https://doi.org/10.1002/jrs.1797.
[30] C.A. Teixeira dos Santos, R.N.M. Páscoa, P.A.L.S. Porto, A.L. Cerdeira, J. M. Gónzalez-Sáiz, C. Pizarro, J.A. Lopes, Raman spectroscopy for wine analyses: A comparison with near and mid infrared spectroscopy, Talanta 186 (2018) 306–314, https://doi.org/10.1016/j.talanta.2018.04.075.
[31] A. Villar, S. Fernandez, E. Gorritxategi, J.I. Ciria, L.A. Fernandez, Optimization of the multivariate calibration of a Vis-NIR sensor for on-line monitoring of marine diesel engine lubricating oil by variable selection methods, Chemom. Intel. Lab. Syst. 130 (2014) 68–75, https://doi.org/10.1016/j.chemolab.2013.10.008.
[32] A. Villar, J. Vadillo, J.I. Santos, E. Gorritxategi, J. Mabe, A. Arnaiz, L.A. Fernandez, Cider fermentation process monitoring by Vis-NIR sensor system and chemometrics, Food Chem. 221 (2017) 100–106, https://doi.org/10.1016/j.foodchem.2016.10.045.
[33] A. Virga, P. Rivolo, E. Descrovi, A. Chiolerio, G. Digregorio, F. Frascella, M. Soster, F. Bussolino, S. Marchio, F. Geobaldo, F. Giorgis, SERS active Ag nanoparticles in mesoporous silicon: detection of organic molecules and peptide-antibody assays, J. Raman Spectrosc. 43 (2011) 730–736, https://doi.org/10.1002/jrs.3086.
[34] N.R. Yaffe, E.W. Blanch, Effects of anomalies that can occur in SERS spectra of biological molecules when using a wide range of aggregating agents for hydroxylamine-reduced and citrate-reduced silver colloids, Vib. Spectrosc 48 (2008) 196–201, https://doi.org/10.1016/j.vibspec.2007.12.002.
[35] K. Yoshikawa, Y. Uekusa, A. Sakuragawa, Determination of sulfite in wines using suppressed ion chromatography, Food Chem. 174 (2014) 387–391, https://doi.org/10.1016/j.foodchem.2014.11.066.
[36] W. Yue, T. Gong, X. Long, V. Kravets, P. Gao, M. Pu, C. Wang, Sensitive and reproducible Surface-Enhanced Raman Spectroscopy (SERS) with arrays of dimer-nanopillars, Sens. Actuators B 322 (2020), 128563, https://doi.org/10.1016/j.snb.2020.128563.
[37] H. Wang, Y. Wu, H. Song, Synergistic effects of photonic crystal and gold nanostars for quantitative SERS detection of 3-Phenoxybenzoic acid, Appl. Surf. Sci. 476 (2019) 587–593, https://doi.org/10.1016/j.apsusc.2019.01.061.

[38] Q. Wang, Z. Li, Z. Ma, L. Liang, Real time monitoring of multiple components in wine fermentation using an on-line auto-calibration Raman spectroscopy, Sens. Actuators B 31 (2014) 426–432, https://doi.org/10.1016/j.snb.2014.05.109.
[39] F. Westad, H. Martens, Variable selection in Near Infrared spectroscopy based on significance testing in partial least squares regression, J. Near Infrared Spectrosc. 8 (2000) 117–124, https://doi.org/10.1255/jnirs.271.
[40] L. Wu, W. Wang, W. Zhang, H. Su, Q. Liu, J. Gu, T. Deng, D.i. Zhang, Highly sensitive, reproducible, and uniform SERS substrates with a high density of three-dimensionally distributed hotspots: Gyroid-structured au periodic metallic materials, NPG Asia Mater. 10 (1) (2018) e462, https://doi.org/10.1038/am.2017.230.
[41] H. Xu, J. Aizpurua, M. Käll, P. Apell, Electromagnetic contributions to single-molecule sensitivity in surface-enhanced Raman scattering, Phys. Rev. E 62 (3) (2000) 4318–4324, https://doi.org/10.1103/PhysRevE.62.4318.
[42] M. Zhao, Y. Li, Simple methods for rapid determination of sulfite in food products, Food Control 17 (2006) 975–980, https://doi.org/10.1016/j.foodcont.2005.07.008.
[43] V.J. Smith, Determination of sulfite using a sulfite oxidase enzyme electrode, Anal. Chem. 59 (1987) 2256–2259, https://doi.org/10.1021/ac00145a010.
[44] K.H. Esbensen, B. Swarbick, Multivariate data analysis. An introduction to multivariate analysis, process analytical technology and quality by design, sixth ed.,, CAMO Software AS, Oslo, 2018.

Further reading

[20] J.P. Perdew, Density-functional approximation for the correlation energy of the inhomogeneous electron gas, Phys. Rev. B 33 (1986) 8822–8824, https://doi.org/10.1103/PhysRevB.33.8822.